Developing Low-Power Transceiver Technologies for In Situ Communication Applications

N. Lay,[1] C. Cheetham,[1] H. Mojaradi,[1] and J. Neal[1]

For future deep-space missions, significant reductions in the mass and power requirements for short-range telecommunication systems will be critical in enabling a wide variety of new mission concepts. These possibilities include penetrators, gliders, miniature rovers, balloons, and sensor networks. The recent development activity reported in this article has focused on the design of ultra-low-mass and -power transceiver systems and subsystems suitable for operation in a flight environment. Under these efforts, the basic functionality of the transceiver has been targeted towards a Mars microprobe communications scenario. However, the overall transceiver architecture is well suited to any short- or medium-range application where a remote probe will aperiodically communicate with a base station, possibly an orbiter, for the eventual purpose of relaying science information back to Earth. Additionally, elements of the radio architecture can be applied in situations involving surface-to-surface communications, thereby enabling different mission communications topologies. Through a system analysis of these channels, both the applicability and benefit of very low power communications will be quantitatively addressed.

I. Introduction

The development of telecommunications equipment emphasizing very low power consumption and mass will be a significant enabler of future in situ missions with highly constrained payload resources. The activities reported in this article began as a follow-on and complementary effort of the Micro Communications and Avionics Systems first prototype (MCAS1) [1]. The baseline transceiver concept, under this effort, has been oriented towards a Mars microprobe-type mission that would deploy to the surface, gather science, and await opportunities for return-link data transmissions to a low-altitude polar orbiter, as shown in Fig. 1. It is envisioned that such a mission would be characterized by communications to an orbiting satellite with local relay capability, where the communications duration and frequency would be driven by return-link opportunities coupled with science data collection requirements. Under such a scenario, receiver power consumption is a critical parameter in determining mission duration, and any significant improvements in this arena will have a direct benefit on the mission's longevity. Consequently, a principal focus of the development activity has been to design and demonstrate a low-complexity, low-

[1] Communications Systems and Research Section.

The research described in this publication was carried out by the Jet Propulsion Laboratory, California Institute of Technology, under a contract with the National Aeronautics and Space Administration.

power receiver architecture capable of meeting this application. Furthermore, future needs for short-range surface communications, as depicted in Fig. 1, would also benefit from such a transceiver.

This article is organized in the following manner. In Section II, we quantitatively describe a number of Mars-oriented communications links from the standpoint of required RF power consumption. These discussions provide insights into the benefits of low-power telecommunications electronics to applications beyond the microprobe–orbiter scenario. Both short-range and long-range surface links are considered. In Section III, we describe the transceiver architecture, the specifics of receiver and transmitter designs, and the quantitative benefits of reducing the power consumption of the telecommunications electronics for the communications scenarios examined in Section II. In addition, the status of current and future developments will also be reviewed.

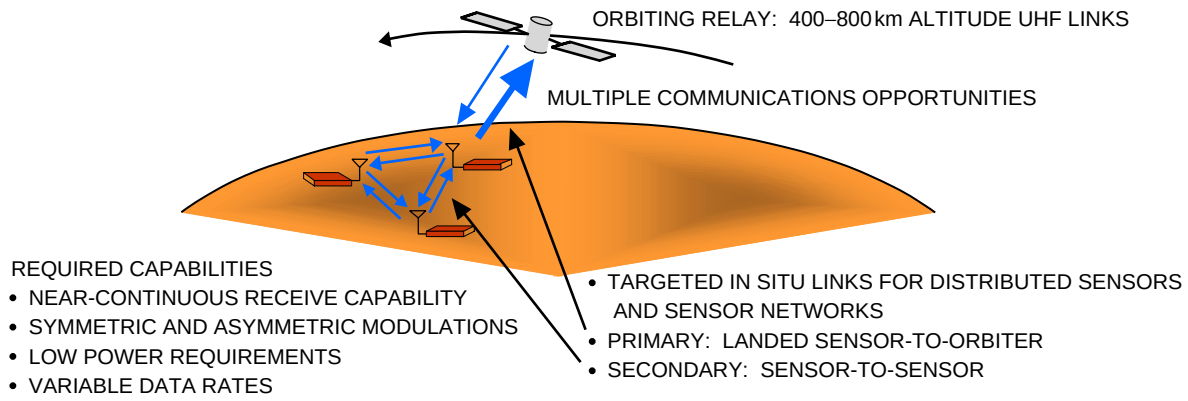

Fig. 1. Example microprobe and distributed sensor communications scenarios.

II. Applications

In this section, we examine communications links arising from various in situ mission scenarios. These links can be broadly categorized as communications between an orbiter and a surface element or as communications between the surface elements themselves. This would include ground-to-ground signaling (of relevance to landers, miniature rovers, and sensor networks) and "air"-to-ground transmissions (of relevance to gliders, airplanes, and balloons). Both categories of links are primarily evaluated in terms of RF power requirements for a given bit-error rate (BER), parameterized by variables such as data rate, range, and altitude. Parameters for these links, such as lander–orbiter slant range, are consistent with planned or potential Mars-based communications scenarios. Furthermore, some choices in signal design (e.g., frequency, modulation, and coding) assume the existence of orbiting telecommunications assets, primarily for purposes of data relay back to Earth. By evaluating these scenarios based on power requirements, we can quantify data-link capabilities (throughput and range) corresponding to lower-power transmitters (10–1000 mW) that would be consistent with highly miniaturized, low-power telecommunications.

A. Orbiter–Surface Links

For the microprobe mission scenario, free-space propagation loss, low-gain omni-directional antennas, and operation at UHF frequencies in the 400-MHz range characterize the communications link parameters. The choice of UHF operation for links anchored by low-gain antennas is motivated by two factors: (1) reduced free-space losses compared to alternative frequencies [e.g., 2 GHz (S-Band)] and (2) interoperability with current and future missions.

Tables 1 and 2, respectively, provide example link budget details for forward- and return-link communications between a low-altitude polar-orbiting relay and a landed surface probe. The format and numerous parameter values, such as link frequencies, nominal losses, equivalent temperature, noise figure, etc., have been summarized from more detailed versions taken from various sources.[2,3] The communications range

Table 1. Orbit-to-surface command/hailing link budget.

Parameter	Value
Orbiter transmitter	
Transmitter power	30 dBm
Transmitter circuit losses	−1.0 dB
Antenna gain	0.0 dB
Link	
Range	894.3 km
Link frequency	437.1 MHz
Space losses	−144.28 dB
Microprobe receiver	
Antenna gain	0.0 dB
Polarization losses	−0.2 dB
Receiver circuit losses	−1.0 dB
Receiver noise figure	3.0 dB
System noise temperature	600 K
Noise spectral density	−170.9 dBm/Hz
Total power summary	
Received power	−116.48 dBm
Received C/N_o	54.42 dB
Data-channel performance	
Data bit rate	1000 b/s
E_b/N_o to receiver	24.42 dB
Implementation loss	2.0 dB
Effective E_b/N_o	22.42 dB
Uncoded BPSK performance margin	11.82 dB
Uncoded DPSK performance margin	11.62 dB
Uncoded FSK performance margin	8.22 dB

[2] D. Hansen, *MCAS1 Functional Requirements*, draft (JPL internal document), Jet Propulsion Laboratory, Pasadena, California, October 1999.

[3] D. Hansen and M. Sue, *Frequency Bands for Local Communication and Navigation in the Mars Region*, (JPL internal document), Jet Propulsion Laboratory, Pasadena, California, January 31, 2001.

Table 2. Surface-to-orbit link budget.

Parameter	Value
Microprobe transmitter	
Transmitter power	26 dBm
Transmitter circuit losses	−1.0 dB
Antenna gain	0.0 dB
Link	
Range	894.3 km
Link frequency	401.5 MHz
Space losses	−143.55 dB
Orbiter receiver	
Antenna gain	0.0 dB
Polarization losses	−0.2 dB
Receiver circuit losses	−1.0 dB
Receiver noise figure	3.0 dB
System noise temperature	600 K
Noise spectral density	−170.9 dBm/Hz
Total power summary	
Received power	−119.75 dBm
Received C/N_o	51.15 dB
Data-channel performance	
Data bit rate	20,000 b/s
E_b/N_o to receiver	8.14 dB
Implementation loss	1.5 dB
Effective E_b/N_o	6.64 dB
(7,1/2) convolutionally coded BPSK performance margin	2.04 dB
(2048,1024) turbo-coded BPSK performance margin	4.14 dB

selected in these tables corresponds to the slant path for a 400-km altitude, polar-orbiting satellite situated at an effective elevation angle of 20 deg relative to the surface transceiver. As a point of reference, the theoretical additive white Gaussian noise (AWGN) E_b/N_0 thresholds, corresponding to a BER of 10^{-6}, for possible forward- and return-link modulation and coding choices are presented in Table 3 [2,3].

A representative forward-link data rate of 1000 b/s is shown and assumed sufficient for the purpose of having an orbiter individually alert multiple landed elements of return-link opportunities during a single pass. In addition, the forward link may also be employed to deliver operational or science-gathering

Table 3. Ideal E_b/N_o thresholds for various types of modulation and coding, BER = 10^{-6}.

Modulation and coding	Required E_b/N_o, dB
Uncoded coherent BPSK	10.6
Uncoded non-coherent FSK	14.2
Uncoded differentially coherent BPSK	10.8
Coherent BPSK with (7,1/2) convolutional code	4.6
Coherent BPSK with (2048,1024) turbo code	2.5

commands to these elements. Transmitter RF power for the forward link is nominally set to 1 W,[4] with the assumption that this could be readily increased for most orbital payloads. The command-link margins are given for three different uncoded modulation and detection types—coherent binary phase-shift keying (BPSK), differentially coherent binary phase-shift keying (DPSK), and non-coherent frequency-shift keying (FSK). Uncoded modulations are selected on the forward link to minimize microprobe receiver complexity. Based on the moderately large margins shown in Table 1, the use of forward error correction (FEC) would indeed not be required to close the command link for this specific scenario, and some measure of receiver implementation loss could be incurred if it resulted in reduced power consumption. Furthermore, even holding the margin constant, increased range could also be achieved through data-rate reductions. The actual choice of modulation can then be made on the basis of simplifying the receiver and reducing its power consumption as well as taking into consideration what forward-link signals will be supported by current and future orbiter missions. Reductions in receiver power consumption directly translate to improved mission longevity when the experiment configuration calls for semi-continuous[5] operation to await random access commands from an orbiter.

A transmitter output power of 400 mW and data rate of 20 kb/s are used in the return-link example of Table 2 and are shown to be sufficient for reliable communications given the use of either the (7,1/2) convolutional code or rate-1/2, 1024-bit block turbo code. The use of FEC on this link is strongly warranted in order to reduce the output power amplifier requirements as much as possible. To determine if reduced power consumption in transmitter electronics (exclusive of the RF power amplifier) can impact overall savings, we will expand upon the results of Table 2 by parametrically calculating transmitter power requirements. This is achieved by fixing the (7,1/2) convolutional code and then varying the return-link data rate and the slant-path range to generate the corresponding transmit RF signal powers for a 3-dB margin. These results are respectively and compactly shown in Figs. 2 and 3 for slant ranges corresponding to low-altitude (polar-orbiting) and high-altitude (areostationary) telecommunications relay links. In Fig. 2, the data rates span 1–100 kb/s, and the link distance ranges from 100 to 2000 km. The color bar shown on the right-hand side of the figure describes the quantitative mapping between transmitter power (dBm) and the plotted color contours. From these results, we note that transmitter powers under 1 W will be able to support 100-kb/s data rates over much of a 400-km-altitude relay's orbit[6] and will support 40 kb/s over the relay's *full* orbit.[7] Note that these plots do not consider elevation-angle-based antenna gain dependencies. In practice, extreme slant ranges for a given orbit will require somewhat more power due to low horizon gain for the surface element's antenna.

[4] Comparable to the 1.3-W UHF forward link on Mars Global Surveyor.

[5] It is assumed that commonly used power-reduction techniques such as low duty cycle operation will also be applied.

[6] Defined as elevation angles greater than 30-deg elevation and less than 700-km range.

[7] Defined as elevation angles greater than 20-deg elevation and less than 900-km range.

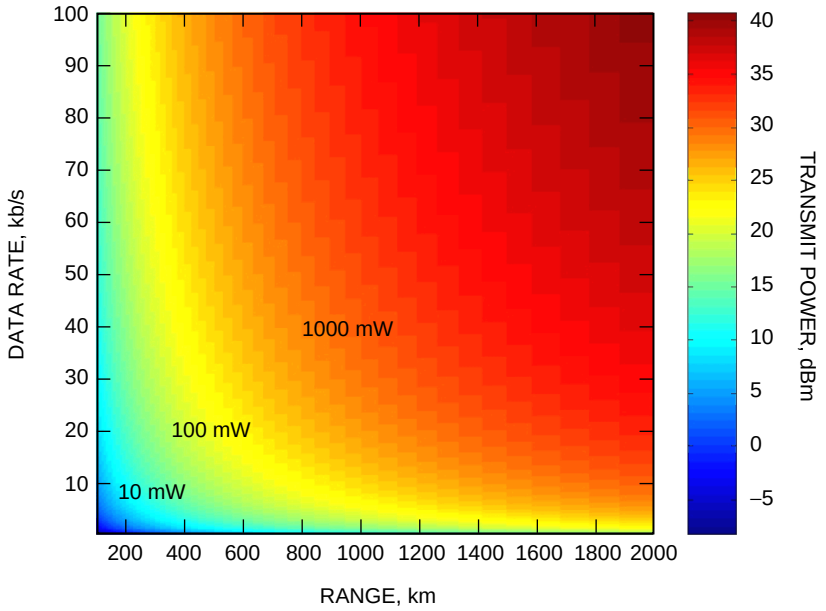

Fig. 2. Low-altitude (100–2000 km) orbiter uplink RF power requirements, coherent BPSK, (7,1/2) convolutional coding.

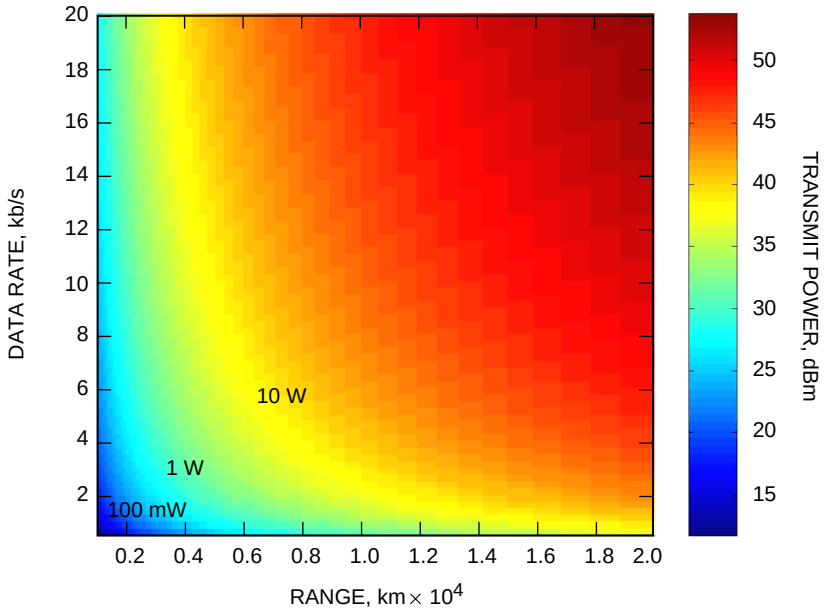

Fig. 3. High-altitude (1000–20,000 km) orbiter uplink RF power requirements, coherent BPSK, (7,1/2) convolutional coding.

In contrast, a communications link between the martian surface and a relay in areosynchronous orbit would experience communications ranges of 17,000 to 20,000 km. At these distances, a transmitter power of 10 W would be required simply to achieve a reliable 1-kb/s link. Mass and volume considerations aside, a higher-gain antenna could be employed on the orbiter to raise the data rate and/or lower transmit power requirements. However, given the dominance of the return-link RF amplifier power consumption, even a modified version of this scenario is unlikely to benefit significantly from power reductions in the transmitter electronics. Both low- and high-altitude orbiter results are discussed in greater detail in Section III. For

both of these figures, we are able to produce the corresponding in situ turbo code results by applying a 2.1-dB reduction in required transmitter power.

B. Surface Links

For surface links, we consider two different communications scenarios corresponding to short-range ground-to-ground and longer-range "air"-to-ground communications. The following analyses address only large-scale propagation models for these channels. The small-scale effects that produce stochastically modeled signal variability, such as shadowing and multipath fading, are not factored into these evaluations. Low-gain antennas are assumed at both the transmitter and the receiver for all surface-link channels discussed.

For the short distances, low antenna heights, and non-line-of-sight paths that characterize communications between small surface elements (e.g., distributed sensors or microrover fleets), the UHF signal propagation model[8] consists of two loss terms:

$$L_{\text{total}} = L_{\text{two ray}} + L_{\text{knife edge}} \tag{1}$$

One corresponds to a two-ray (line-of-sight and reflected ground path) model and the other to a knife-edge diffraction model. Pictorial descriptions of these models are respectively shown in Figs. 4 and 5. The two-ray model accounts for signal attenuation over flat terrain,

$$L_{\text{two ray}} = \frac{h_{tx}^2 \times h_{rx}^2}{D^4} \tag{2}$$

while the knife-edge model incorporates losses due to intervening obstacles. The special-case loss corresponding to a single diffracting obstacle located equidistantly between transmitter and receiver is given by

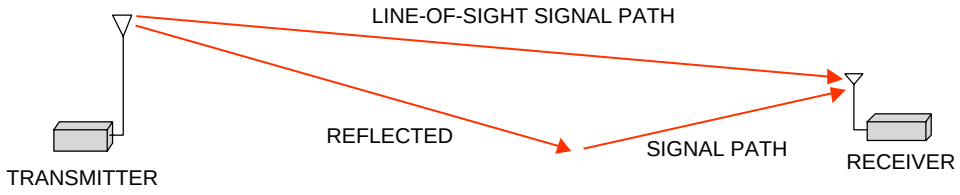

Fig. 4. Two-ray surface propagation model.

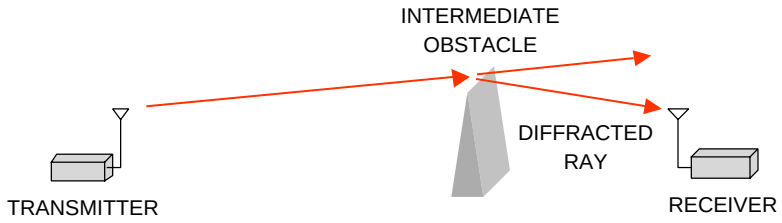

Fig. 5. Knife-edge diffraction propagation model.

[8] E. Satorius, *Overview of Propagation Models and Data Analysis Methods*, Report prepared for Army Research Lab under JPL Task Order RF-182, Amendment No. 855 (internal document), Jet Propulsion Laboratory, Pasadena, California, May 11, 1998.

$$L_{\text{knife edge}} = \begin{cases} 0, & \nu \leq -1 \\ (0.5 - 0.62 \times \nu)^2, & -1 < \nu \leq 0 \\ \left(0.5 \times e^{-0.95\nu}\right)^2, & 0 < \nu \leq 1 \\ \left(0.4 - \sqrt{0.1184 - (0.38 - 0.1 \times \nu)^2}\right)^2, & 1 < \nu \leq 2.4 \\ \left(\dfrac{0.225}{\nu}\right)^2, & \nu > 2.4 \end{cases} \tag{3}$$

where

$$\nu = h_{\text{obstacle}} \times \sqrt{\frac{8}{\lambda \times D}}$$

Using these models, we can plot the required transmitter power to support a low-data-rate link as functions of range and obstacle height. The low-data-rate, surface-to-surface application is meant to illustrate an adjunct capability to the basic microprobe transceiver that could enable new means of collaborative science gathering through short-range connectivity. Assuming the use of a low-complexity command receiver optimized for minimal power consumption, a 1-kb/s data rate, non-coherent FSK modulation, and transmit and receive antenna heights of 1/2 m, we arrive at the results shown in Fig. 6. For transmitter output powers under 1 W, a communications range of 1.5 to 2.5 km can be achieved even with intervening obstacles ranging from 2 to 20 m above the antenna heights. These results suggest that the incorporation of a simple FSK modulator in the return-link transmitter would easily add a low-rate communications capability to allow networking between several landed elements in close proximity.

For additional insight, we also consider the use of a high-performance error-correcting code coupled with coherent detection (BPSK, turbo coding) applied to the short-distance surface channel. For a presumed increase in receiver complexity and corresponding power consumption, this configuration achieves the results shown in Fig. 7. For the 1-kb/s throughput, a range of 2 to 3 km can be maintained while

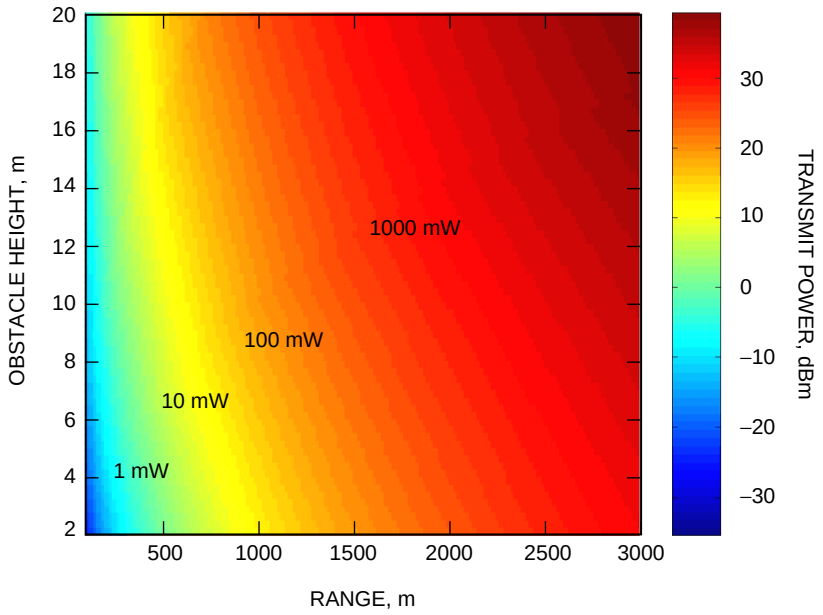

Fig. 6. Short-range (100–3000 m) ground-to-ground RF power requirements, 1 kb/s, uncoded non-coherent FSK, 0.5-m antenna heights.

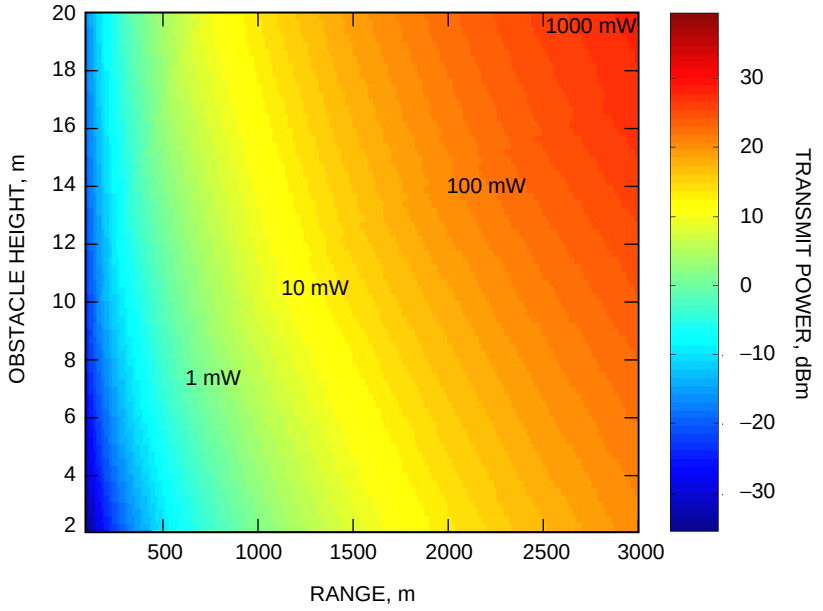

Fig. 7. Short-range (100–3000 m) ground-to-ground RF power requirements, 1 kb/s, turbo-coded coherent BPSK, 0.5-m antenna heights.

expending less than 100 mW of transmitter output power. Such a significant relative improvement could be exploited in a ground communications scenario with a higher power consumption relay terminal configured as the central point of a star network topology in much the same role the orbiter assumes in relation to surface-based microprobes.

Next, we consider the RF transmit power requirements for high-data-rate, "airborne" transmitter-to-surface communications channels. This scenario will be highly relevant to missions involving communications from an elevated platform (e.g., glider, powered aircraft, balloon, etc.) to a ground-based relay. The high-data-rate application will be particularly suited to imager-based science measurements, and the ground-based relay can serve as a hub for multiple long-range missions without suffering the inconstancy of a link to an orbiter. Under this configuration, we are interested in minimizing the power consumption on the transmitter side, as these platforms will likely exhibit severe payload power, mass, and volume constraints. Such a focus will naturally argue for the use of FEC and coherent detection, which will consequently impose additional complexity on the ground-based relay.

For these calculations, the gross propagation losses are modeled as a combination of square-law free-space losses and fourth-power ground-wave models where the individual loss functions are

$$\left.\begin{aligned} L_{\text{free space}}(D) &= \left(\frac{\lambda}{4\pi D}\right)^2 \\ L_{\text{two ray}}(D) &= \frac{h_{tx}^2 \times h_{rx}^2}{D^4} \end{aligned}\right\} \tag{4}$$

The crossover point between these two expressions can be determined by setting the two functions equal and solving for the range:[9]

[9] E. Satorius, personal communication, Jet Propulsion Laboratory, Pasadena, California, May 4, 2001.

$$L_{\text{free space}} = L_{\text{two ray}} \Rightarrow D_{\text{crossover}} = \frac{4\pi \times h_{tx} \times h_{rx}}{\lambda} \tag{5a}$$

therefore,

$$L_{\text{channel}} = \begin{cases} L_{\text{free space}}(D), & D \le D_{\text{crossover}} \\ L_{\text{free space}}(D_{\text{crossover}}) \times L_{\text{two ray}}(D - D_{\text{crossover}}), & D > D_{\text{crossover}} \end{cases} \tag{5b}$$

For example, given transmitter altitudes of 2 and 5 km, a receiver antenna height of 1 m, and a 400-MHz carrier frequency, the crossover point occurs at 33.5 and 83.4 km, respectively, from the transmitter. It should, however, be noted that these results were computed assuming a purely flat Mars surface model and at large slant ranges will be optimistic in comparison with a model that accounts for planet curvature.

In Figs. 8 and 9, the required transmitter power is plotted as a function of range and received antenna height for transmitter altitudes of 2 and 5 km, with convolutionally coded (7,1/2) BPSK and a data rate of 1 Mb/s. Received antenna heights are allowed to vary from 1 to 5 m, and the slant path ranges up to 100 km.

Over much of the parameter space of Fig. 8 (2-km transmitter altitude), the free-space path-loss function dominates the overall loss equation. Only at large slant ranges and lower received antenna heights (lower right portion of the figure) does the increased transmitter power requirement exhibit the two-ray loss mechanism. In this region, the RF power requirement rises to the 1-W level in order to close the link for slant paths nearing 100 km. At the higher 5-km altitude, the free-space path-loss rule dominates nearly all of Fig. 9, illustrating that on the order of 25–26 dBm (∼300–400 mW) is sufficient to downlink high-rate telemetry over the considerable distance of 100 km, provided a certain altitude is achieved. However, several other practical factors will also impact the communications performance across such a link. Because of the low elevation angle at extreme ranges, these factors will include blockage due to local geography and frequency-selective multipath due to the high-data-rate transmission. Both of these effects can be partially mitigated by increasing the receiver antenna height—either through mechanical augmentation or by locating the receiver on high ground. In addition, as observed in Figs. 8 and 9,

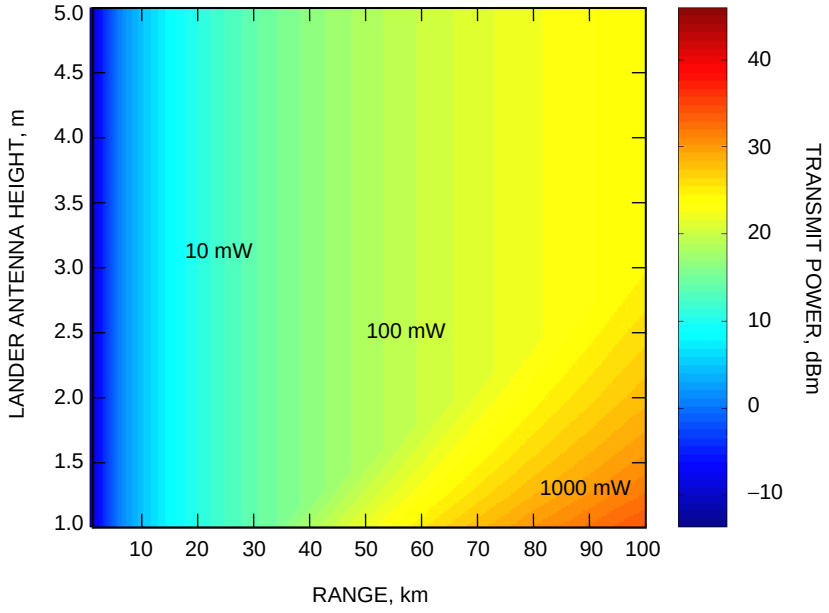

Fig. 8. "Air"-to-surface RF power requirements, 1 Mb/s, transmitter altitude 2000 m.

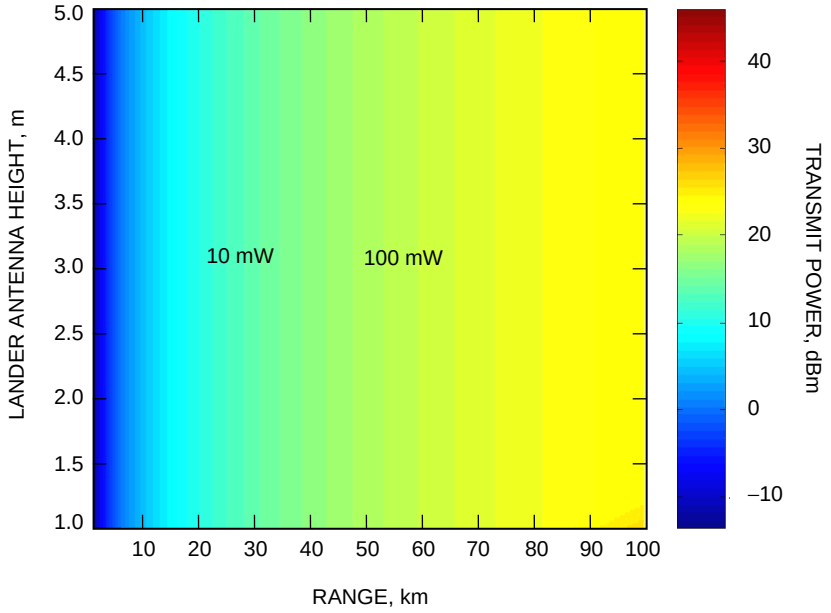

Fig. 9. "Air"-to-surface RF power requirements, 1 Mb/s, transmitter altitude 5000 m.

this also has the effect of increasing $D_{\text{crossover}}$, the free-space path-loss slant range, thereby substantially lowering transmit power requirements. Although significant mass, mechanical design, or operational constraints would accompany efforts to locate the receiver antenna in as high a position as possible, given its highly beneficial impact, it would be considerably worthwhile to address this area of improvement during system and receiver design phases of any future mission.

III. Transceiver Description

In this section, we describe the architecture of a low-power transceiver that is predicated upon reasonable trade-offs of functionality and performance to achieve certain power-consumption targets. Before launching into a detailed description, some commentary is warranted regarding what constitutes "low-power" operation and what consumption targets would be both feasible and worthy of development. In pursuing this development, we have tailored our approach based on the following objectives: (1) achieving significantly reduced power consumption (∼10 times lower) compared to previous developments targeting in situ needs,[10] (2) primarily targeting receiver power consumption as most relevant to increased mission longevity, and (3) limiting the modulator electronics to a small fraction of total required transmitter power. In terms of absolute numbers, these guidelines result in a power consumption target range of 20 to 50 mW for all of the receiver or transmitter electronics (power amplifier excluded). While commercial examples of state-of-the-art single-chip transceivers may more than satisfy the power requirements, their communications performance, reliability, and inability to be customized render them ill suited for flight applications.[11] Nonetheless, their existence is a reassurance that the target range can be achieved while taking into account important requirements specific to in situ applications.

In our development, we pursue a staged approach in which we focus on prototyping a functionally complete transceiver using both discrete-component and integrated-circuit designs. In addition, intermediate prototypes are developed as miniaturized assemblies suitable for rapid infusion. As we continue

[10] For example, Mu Space Engineering Spacecraft (MUSES-CN), Deep Space 2 telecommunications.

[11] N. Lay, *Low Power Transceiver Technologies and Applications for In Situ Communications*, draft (JPL internal document), Jet Propulsion Laboratory, Pasadena, California, July 2000.

with the development, we plan to refine power and performance on a subsystem-by-subsystem basis and replace the functional prototypes with their end products. This approach exhibits the dual virtues of potentially applying intermediate products to near-term missions and continually maintaining a full system test capability throughout the evolution of various transceiver elements.

For the microprobe application, we have developed the following candidate configuration: a half-duplex system with a single-channel non-coherent receiver capability coupled with a transmitter capable of generating FEC-encoded signaling. In Fig. 10, details of such an architecture reveal multiple-transmit-channel capability through the use of a synthesizer and a simple receiver front end consisting of a low-noise amplifier (LNA) and a 1-bit sampler. The additional power required for the frequency synthesizer is assumed to be minor relative to the power consumption of internal or external transmit amplifiers and justified by the additional flexibility afforded by the inclusion of such an element. For both receive and transmit baseband circuits, multi-rate capability is essential as an added degree of freedom in being able to optimize forward and return links for maximum throughput. The following sections provide details of the receiver and transmitter designs and a quantitative analysis of improvements in total transmitter power consumption for several specific communications applications.

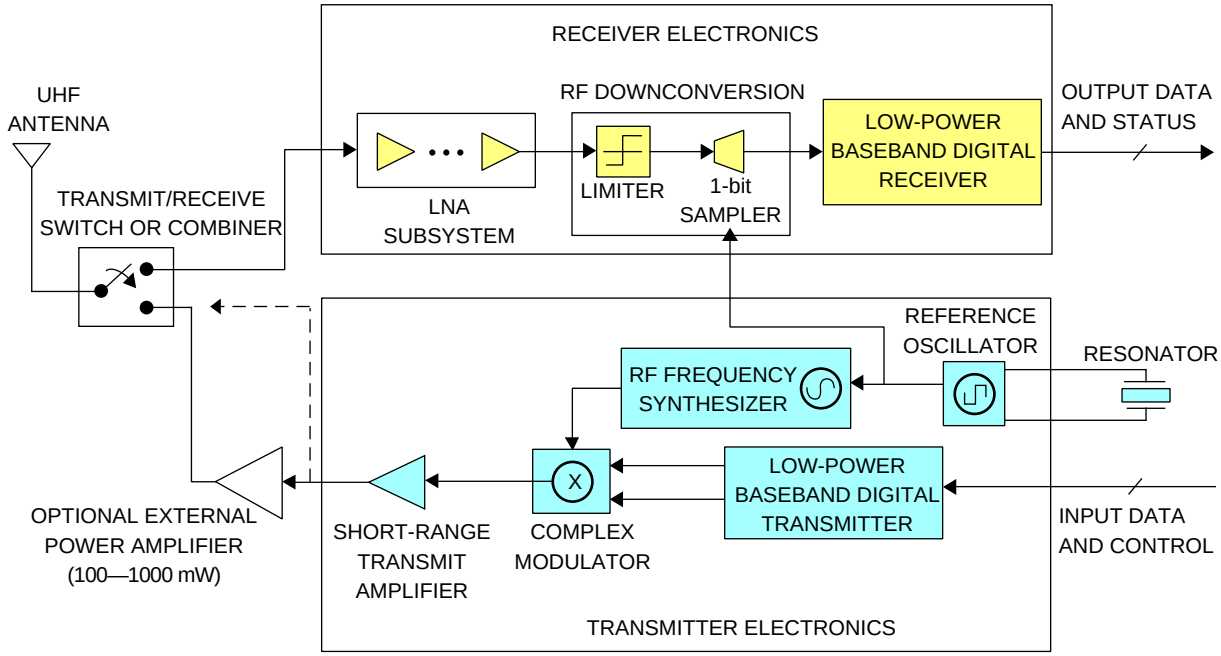

Fig. 10. Transceiver block diagram.

A. Low-Complexity Receiver

In 1999, JPL initiated a study and development contract with the University of California, Los Angeles (UCLA) to investigate and develop a very low power, digital receiver design. The relevant mission scenario corresponded to the demodulation of command signals from a Mars orbiter communicating to a microprobe. The key functional factors under consideration were low speed, multi-rate operation (0.1–10 kb/s), tolerance to large Doppler offsets (±10 kHz), UHF operation (437.1 MHz), absence of in-band interferers, and low power consumption. From this charter, the investigators, Daneshrad and Grayver, developed a conceptual system model [4] and proceeded with a detailed receiver design with an eventual goal of fabrication as an application-specific integrated circuit (ASIC). The fundamental premise of their approach [5–8] is best summarized as follows:

(1) Simplify the front-end architecture to allow digital processing as early as possible in the receiver chain.

(2) Realize as a digital integrated circuit that is easily ported between different fabrication processes.

(3) Utilize complementary metal oxide semiconductor (CMOS) digital processing for low power consumption (proportional to the clock rate).

(4) Select non-coherent detection to avoid acquisition and tracking complexities with coherent systems.

(5) Assume the absence of interferers, allowing 1-bit processing to reduce receiver complexity.

(6) Accept some degradation to achieve the lowest power consumption possible.

Details of the receiver system architecture are shown in Fig. 11. For simplicity, the receiver is designed to operate at a single frequency. The overall system design requires that the front end need perform only low-noise amplification, narrowband bandpass filtering, and subsampling of the carrier signal. The bandpass filtering is based on surface acoustic wave (SAW) filter technology and, for devices operating in the UHF range, are capable of achieving an RF bandwidth of roughly 500 kHz. Based on this bandwidth, 1.2 MHz is the minimum allowable subsampling rate to avoid noise aliasing and enable quadrature sampling of the 437.1-MHz carrier [4,9]. After quadrature sampling and demultiplexing, the 1-bit samples are downsampled by a 24:1 ratio to further lower the CMOS processing rate for power conservation. Depending on the data rate, the signal will be either directly detected (10 kb/s) using a 16-point discrete Fourier transform (DFT) or frequency compensated via direct digital frequency synthesis (DDFS) and further downsampled by factors of ten through one (1 kb/s) or two (100 b/s) stages prior to final DFT detection. Other features incorporated into this design include programmability of the following parameters: modulation index, packet unique word length and value, and thresholds for frequency and timing acquisition.

This design was fabricated through a MOSIS submission using the Taiwan Semiconductor Manufacturing Company's 0.25-μm CMOS process. Preliminary tests indicated basic functional operation for the 10 packaged prototypes delivered from the foundry. The combined core and input/output (I/O) power consumption required by these baseband FSK receivers ranges from 0.6 to 4.3 mW for operating voltages of 1.0 and 2.5 V.

In order to evaluate the performance of the baseband receiver ASIC under realistic command signal conditions, we have initially implemented the required front-end functionality called for in the low-complexity

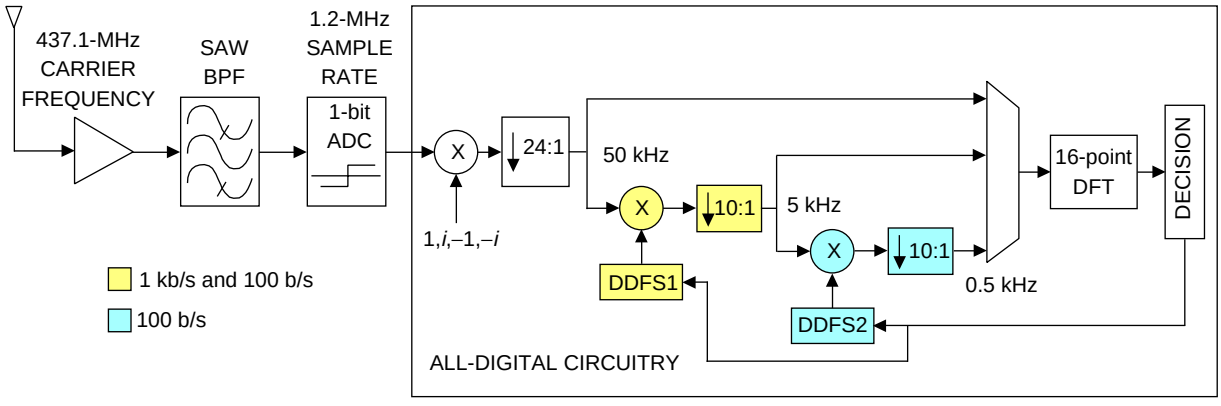

Fig. 11. Low-power receiver functionality.

receiver architecture through a design utilizing discrete commercial off-the-shelf (COTS) components. This includes a six-amplifier high-gain block with two sections of bandpass filtering integrated between several of the gain stages. Wideband gallium arsenide (GaAs) amplifiers and a narrowband (500–700 kHz bandwidth) SAW filter centered at 433.92 MHz form the core components of this subsystem. In Fig. 12, two realizations of the gain and filtering block are shown in which the smaller circuit assembly corresponds to the more advanced and miniaturized version. An 8-bit commercial analog-to-digital converter (ADC) with a front-end bandwidth of 475 MHz follows this circuit. The performance of this front end is currently being evaluated over an input signal level range of −130 to −100 dBm. The digitized outputs are subsampled using the 364.25 ratio called for in the original receiver design and are analyzed using spectral analysis and non-real-time software demodulator tools. Ultimately, the most significant bit (MSB) output of the ADC will be connected to the input of the UCLA chip and tested under relevant sensitivity and Doppler offset conditions. The integrated testing of the front-end prototype and the FSK receiver ASIC will be the subject of a future article.

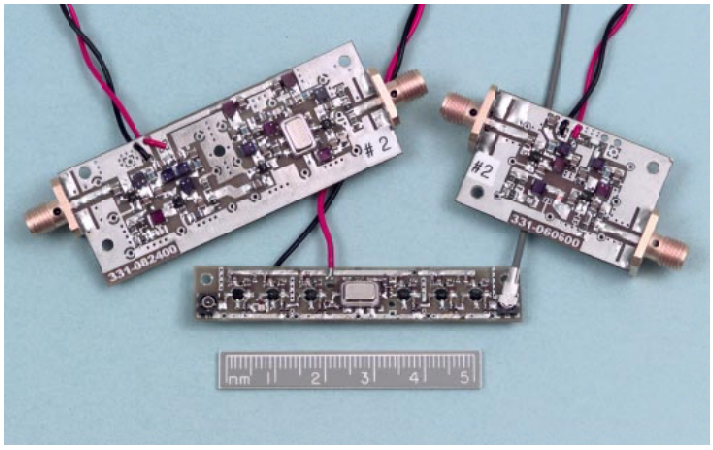

Fig. 12. Miniaturized UHF subsampling front-end prototype: two design iterations of the gain and bandpass circuitry.

B. Miniaturized Transmitter

It has often been generalized that the overall power required to generate a long-range telemetry transmission is dominated by the power amplifier. Given this supposition, an initial implementation of the UHF transmitter subsystem has been realized as a miniaturized, hardware-programmable design based on field programmable gate array (FPGA) and radio frequency integrated-circuit (RFIC) technologies. By pursuing this approach, we are able to develop a low-risk, low-cost subsystem that could be infused in small missions requiring this functionality. The use of a programmable gate array allows for future enhancements and customization in the digital design. A detailed block diagram of the transmitter is shown in Fig. 13. Through the use of inherently radiation-hardened GaAs RFICs (e.g., the complex modulator), components with adequate radiation-testing history (e.g., National LMX2305 phase-locked loop[12]), and a radiation-hardened FPGA (Xilinx XQVR300), this design could, in its own right, be rapidly infused into a flight development.

The digital circuit design implemented within the FPGA consists of two core components. One function handles the interface to the UHF synthesizer by performing transmit channel selection and then programming the phase-locked loop integrated circuit with the appropriate numerical divisors. The approximate range of coverage is 390–440 MHz in steps of 10 kHz. The second function implements baseband data

[12] M. Sandor and S. Agarwal, "FY2000 Component Reliability Screening and Qualification," viewgraph presentation (internal document), JPL Parts and Reliability, Jet Propulsion Laboratory, Pasadena, California, November 1, 1999.

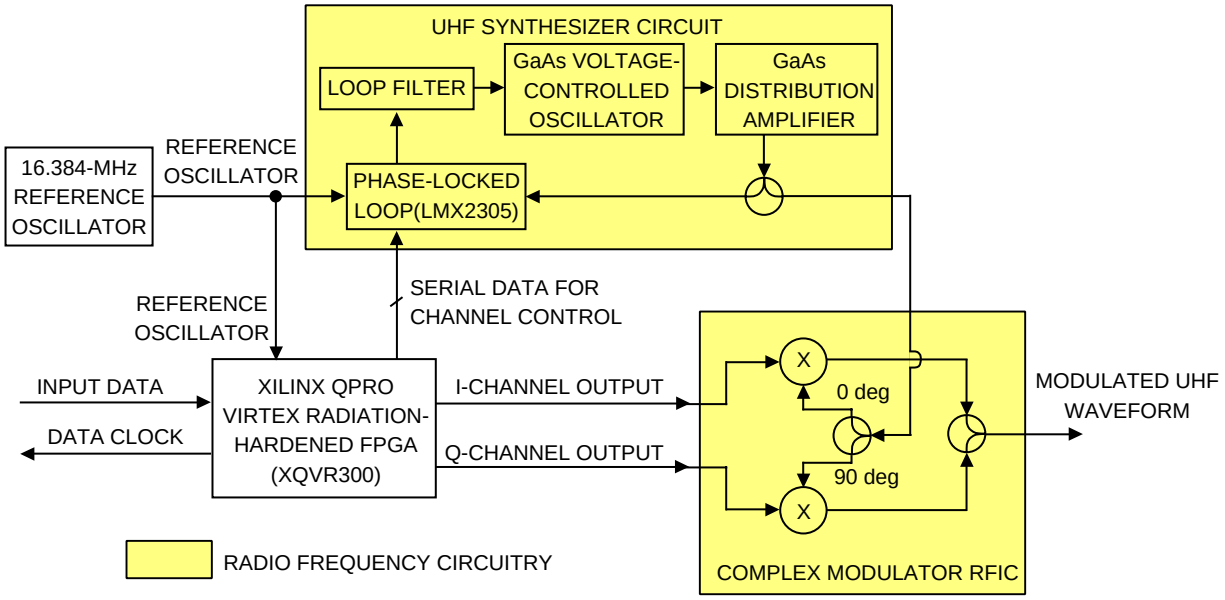

Fig. 13. Miniaturized transmitter block diagram.

formatting to generate digital complex baseband output for various types of transmit waveforms. This design was rapidly integrated through extensive reuse of Verilog code written to implement the MCAS1 modulator circuit [1]. Among its key user-selectable features are the following:

(1) Multi-rate operation ranging from 1 kb/s to 2.048 Mb/s

(2) Residual or suppressed-carrier operation with binary phase-shift keying

(3) V. 35 data scrambling

(4) Differential encoding

(5) Convolutional forward error correction (7,1/2) code

(6) Manchester encoding

In addition, the transmitter's complex baseband outputs from the FPGA will also allow for the generation of both quadrature-phase-shift keying (QPSK) and FSK (albeit with harmonic sidebands) for future expansion. The overall digital design currently occupies a small percentage of the FPGA capacity, thereby leaving sufficient room for any number of near-term augmentations, such as the inclusion of a short-block-length turbo encoder. The development of designs written in Verilog also facilitates their reuse when porting to an eventual low-power ASIC solution.

Photographs of the single-sided RF and digital circuit assemblies are shown in Figs. 14 and 15. The RF circuit card consists of an integrated UHF synthesizer and complex modulator with dimensions of 70×42 mm. The digital card primarily consists of the FPGA and supporting circuitry and interfaces to the RF subsystem and to an external controller. Its dimensions are 72×73 mm. The board layout has also been designed to accommodate both commercial and flight packages of the Xilinx XV300 part. This flexibility will allow populating of the board with the low-cost commercial FPGA for design prototyping activities and reuse of the same layout for a product requiring the radiation-hardened component. Considerable usage of surface-mount technology results in a well-miniaturized overall system and represents the approximate size limits achievable with discrete-component designs. When integrated, the cards will have their non-component sides facing one another.

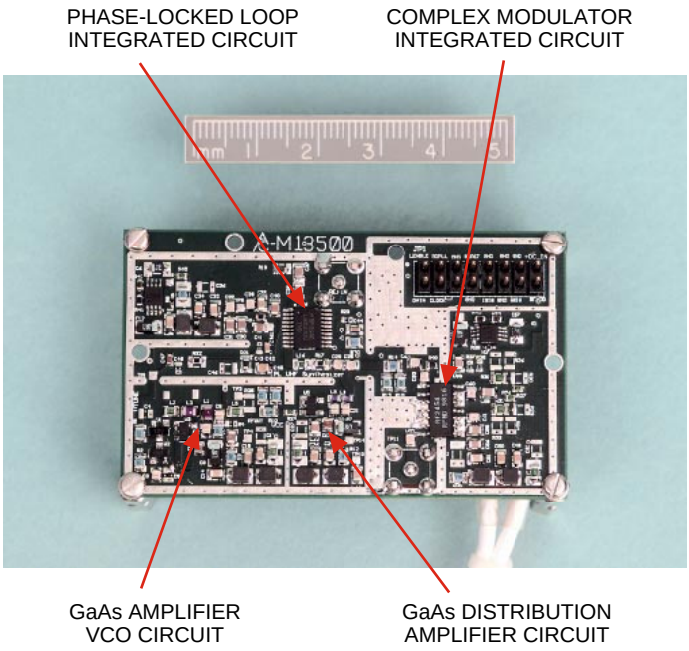

Fig. 14. Transmitter RF circuitry: integrated UHF synthesizer and complex modulator.

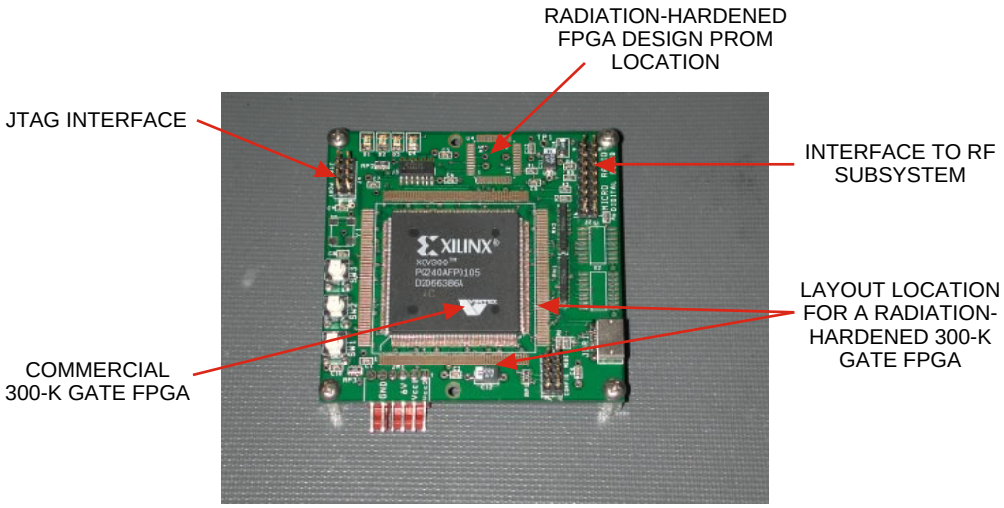

Fig. 15. Transmitter digital circuitry: programmable FPGA. (JTAG is the Joint Test Action Group; PROM is programmable read-only memory.)

C. Power Consumption Benefits

While the benefits of reducing the receiver's power consumption can be clearly understood as a directly proportional increase in operating time given a finite energy supply such as a battery, the equivalent calculation for benefits on the transmitter side are not as straightforward. Therefore, in this section, we will provide a quantification of the overall system benefits that result from reductions in power consumption of the transmitter electronics. Table 4 delineates the power consumption associated with the discrete-component design described in the previous section. The RF circuitry power consumption corresponds to laboratory measurements, and the reference oscillator figure is based on a component survey. The digital

Table 4. Discrete RF transmitter circuit power requirements (power amplifier excluded).

Transmitter circuit element	Estimated power consumption, mW
Integrated synthesizer and complex modulator	335[a]
Reference oscillator	15[b]
Digital modulator ASIC	20[c]
Total power consumption	370

[a] Measured power consumption of miniaturized transmitter RF circuitry.

[b] From a survey of various commercial temperature-compensated crystal oscillator (TCXO) manufacturers.

[c] Estimate based on approximate gate count of FPGA modulator design.

modulator ASIC consumption corresponds to an extrapolation of the FPGA design implemented as a low-power CMOS integrated circuit. The 370-mW power figure represents the required expenditure to perform bit encoding and formatting, synthesized UHF local oscillator generation, and direct upconversion of digital complex baseband signals, resulting in a modulated signal level of several milliwatts. In the following examples, we compare the discrete design power consumption to our 50-mW goal.

In Figs. 16 and 17, we assess the percentage power savings achieved for surface-to-orbit return-link situations. The parameter space and RF transmit power levels, respectively, correspond to a Mars polar orbiter, Fig. 2, and an areostationary orbiter, Fig. 3. The color map on the right-hand side of the figures provides the legend that relates specific colors to the percentage improvement. We arrive at the results shown in these figures by comparing the total power consumption of the discrete-component design of the modulator electronics versus a complete mixed-signal integrated-circuit solution. Factored into the overall consumption is the power requirement of an RF power amplifier that achieves an efficiency of 35 percent. Clearly, some significant savings can be achieved for the low-altitude orbiter application. Power savings of 30 to 60 percent are achieved over a return-link data-rate range of 10 to 70 kb/s for slant paths of 400 to 900 km. The benefit drops off quickly as both range and rate are increased. This effect is strongly reinforced in Fig. 16, which indicates that negligible benefits ensue for a high-altitude orbiter application.

A similar analysis is performed for the high-rate, 1-Mb/s, "air"-to-ground links previously examined in Figs. 8 and 9. We again determine the benefit of reduced power consumption for a low-power integrated-circuit realization of the modulator's digital and RF electronics. For both 2- and 5-km transmitter altitudes, shown in Figs. 18 and 19, a greater than 50 percent improvement is achieved out to a range of 50 km, and better than 30 percent is obtained out to 100 km, provided that the received antenna heights are maintained above 3 and 1 m, respectively. When the slant range is restricted to 30 km or less, free-space path loss is applicable to both scenarios for all antenna heights, resulting in a very significant benefit of greater than 70 percent power savings.

D. Future Development

Thus far, we have shown the beneficial impact of reducing power consumption for both the receiver and transmitter electronics for several specific Mars in situ communications examples. As discussed in

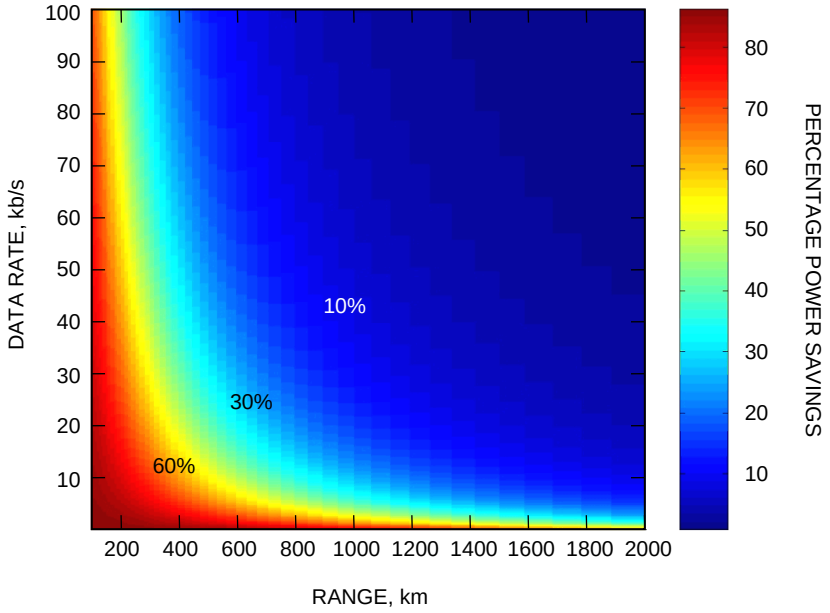

Fig. 16. Total transmitter power savings for low-altitude orbiter links.

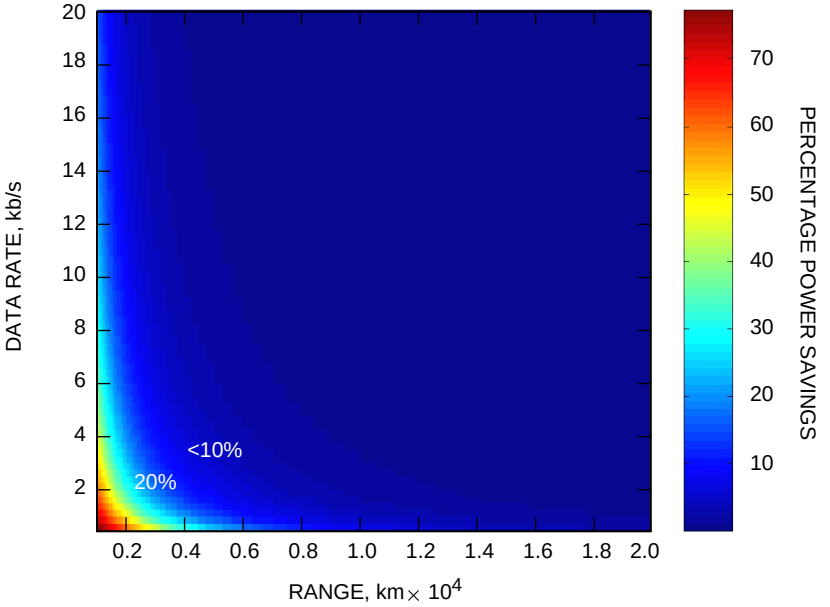

Fig. 17. Total transmitter power savings for high-altitude orbiter links.

previous sections and detailed in Table 4, the bulk of the power draw for current miniaturized telecommunications systems, excluding the transmit power amplifier, is located in the RF circuitry. The next phase of development will directly address this through custom CMOS RFIC design. A review of recent low-power, CMOS-based, RF integrated-circuit designs [10–14] reveals various subsystem (synthesizers, downconverters, etc.) power-consumption figures that are commensurate (tens of milliwatts) with the targets outlined in Section III. Furthermore, the implementation of the RF functionality in CMOS microelectronics will yield additional benefits for future telecommunications equipment, such as large reductions in volume and mass and full integration of RF and digital designs on the same ASIC.

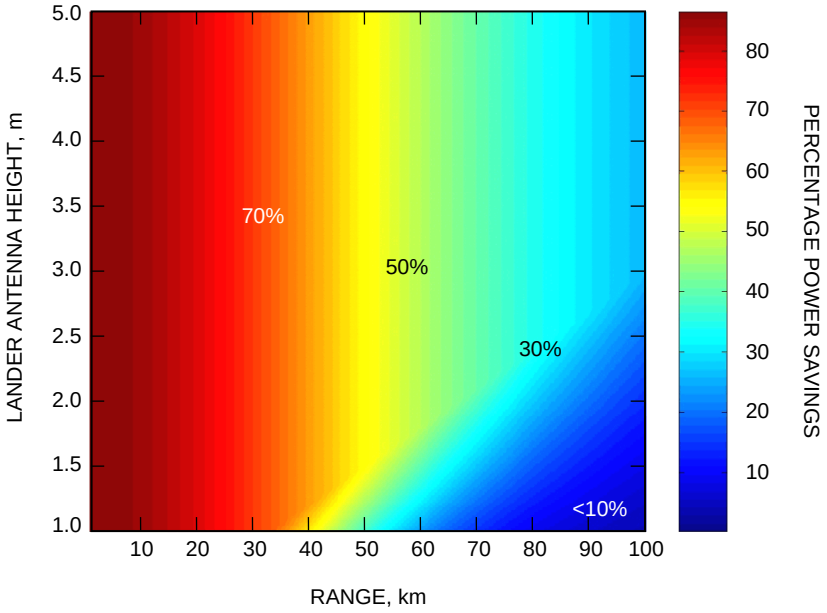

Fig. 18. Total transmitter power savings, 2000-m "airborne" transmitter altitude, 1 Mb/s, (7,1/2) convolutional code.

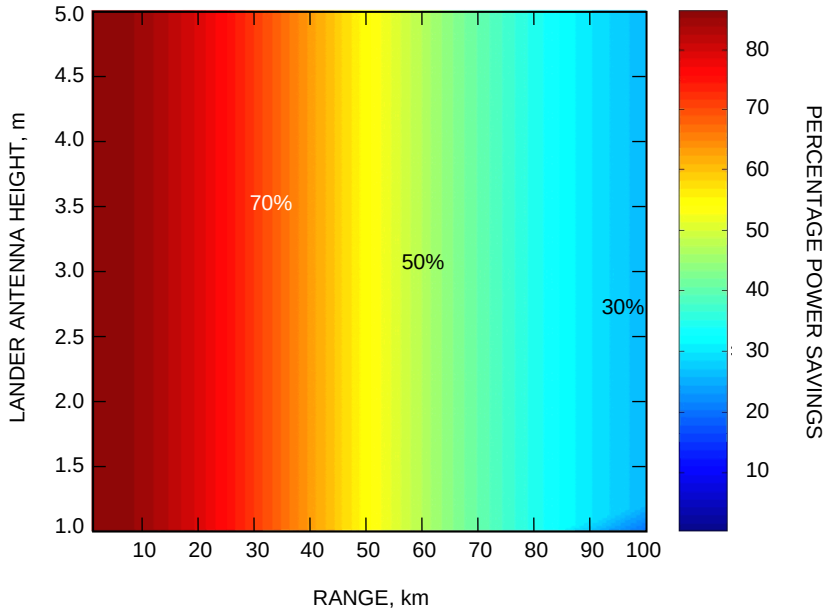

Fig. 19. Total transmitter power savings, 5000-m "airborne" transmitter altitude, 1 Mb/s, (7,1/2) convolutional code.

In order to provide some level of radiation hardening in a CMOS integrated-circuit design, we will target a mixed-signal silicon-on-insulator (SOI) process [15–17]. Two processes represent potential candidates for prototyping small radiation-hardened designs. One is Honeywell's 0.35-μm SOI CMOS approach that is available through a collaboration with the system-on-a-chip program via annual multi-project runs. The second is Peregrine Semiconductor's 0.5-μm silicon-on-sapphire (SOS) approach [17,18] that is available with quarterly multi-project runs through the MOSIS integrated-circuit fabrication cooperative. To date, in FY01, we have initiated LNA RFIC designs targeting the Peregrine process, as it currently appears

to offer greater fabrication opportunities for multiple design iterations during each year. It is anticipated that the high levels of RF and digital integration on radiation-hardened SOI CMOS will ultimately enable new generations of deep-space missions with highly constrained mass and power resources. Furthermore, through modular subsystem development, significant reuse and tailored communications systems solutions should result from these technology investments

IV. Summary

We have described transceiver technology development activities oriented towards very low power telecommunication systems to be used for in situ communications applications. In addition, several quantitative examples of Mars communications scenarios were developed to identify the approximate range and data-rate capabilities associated with this class of telecommunications equipment. These include UHF links between a surface element and an orbiter, and short-range ground-to-ground and longer-range "air"-to-ground configurations.

The use of uncoded modulations and non-coherent detection on the forward polar orbiter-to-lander link was shown to be a viable choice that could simplify the implementation of low-to-medium data rate, low-power consumption command receivers for resource-constrained missions such as a microprobe. The evaluation of surface links further showed that, over relatively flat terrain, low data rates and a range of less than 2 km can be supported with transmitter powers of less than 1 W. In the "airborne" scenario, long distance (approaching 100 km), high-rate, FEC-encoded links of 1 Mb/s can be achieved with several hundred milliwatts of transmit power provided the transmitting "airborne" platform is located at an altitude of several kilometers.

A transceiver architecture targeting the communications link between a surface microprobe and relay orbiter has been developed, and constituent elements of the receiver and transmitter are in various stages of prototyping and functional testing. The current receiver prototype consists of a high-gain, subsampling front end, followed by an ultra-low-power, multi-rate, FSK receiver ASIC fabricated in CMOS technology. The gain and sampling portions of the front end have been realized as a miniaturized, medium-power-consumption, discrete-component design for the purposes of testing the ASIC performance. Initial tests performed on the ASIC confirm its ultra-low-power operation (0.2 to 1.5 mW depending upon supply voltage), and more detailed bit-error-rate tests under relevant channel conditions are planned for completion in the near future. The current transmitter prototype has been developed as a hardware programmable, miniaturized, discrete-component design. The design employs numerous components applicable to a flight regime (e.g., radiation-tolerant or -hardened devices) to enable rapid infusion, in whole or in part, into the development cycle for a suitable mission. To attain very low power consumption for both the transmitter and receiver, the next development phase calls for microelectronic integration of the RF circuitry. Initial receiver front-end design efforts have targeted Peregrine Semiconductor's silicon-on-sapphire (SOS) CMOS as a suitable process for eventual integration of the entire transceiver's RF and digital circuitry, ultimately leading to a radio-on-a-chip implementation suitable for a variety of in situ communication needs.

Acknowledgments

The work described in this article represents the composite compilation of insights and work performed by numerous individuals on a variety of projects. Both detailed and/or informal discussions with each of the following have contributed valuable ideas towards the use and development of highly miniaturized,

low-power transceivers for deep-space applications. These individuals include Babak Daneshrad, Gary Stevens, Martin Agan, Eric Archer, David Bell, Polly Estabrook, Eugene Grayver, Edwin Grigorian, David Hansen, John Huang, Thomas Jedrey, Douglas Price, and Sarita Thakoor.

References

[1] M. Agan, A. Gray, E. Grigorian, D. Hansen, E. Satorius, and C. Wang, "Micro Communications and Avionics Systems First Prototype (MCAS1): A Low Power, Low Mass In Situ Transceiver," *The Telecommunications and Mission Operations Progress Report 42-138, April–June 1999*, Jet Propulsion Laboratory, Pasadena, California, pp. 1–35, August 15, 1999.
http://tmo.jpl.nasa.gov/tmo/progress_report/42-138/138I.pdf

[2] W. Lindsey and M. Simon, *Telecommunication Systems Engineering*, Englewood Cliffs, New Jersey: Prentice Hall, 1973.

[3] J. Odenwalder, *Error Control Coding Handbook*, Final Report, Linkabit Corporation Contract No. F44620-76-C-0056 to U.S. Air Force, distributed by Defense Technical Information Center, July 15, 1976.

[4] E. Grayver and B. Daneshrad, "A Low Power FSK Receiver for Space Applications," *IEEE Wireless Communications and Networking Conference, 2000*, vol. 2, pp. 713–718, 2000.

[5] E. Grayver and B. Daneshrad, "A Self-Contained 100 μW Multirate FSK Receiver ASIC," *IEEE International Solid-State Circuits Conference*, p. 332, 2001.

[6] E. Grayver and B. Daneshrad, "A Low-Power All-Digital FSK Receiver for Space Applications," *IEEE Transactions on Communications*, vol. 49, no. 5, pp. 911–921, May 2001.

[7] E. Grayver and B. Daneshrad, "Direct Digital Frequency Synthesis Using a Modified CORDIC," *IEEE International Symposium on Circuits and Systems*, vol. 5, pp. 241–244, 1998.

[8] E. Grayver, *An Ultra-low-power FSK Receiver for Space and Terrestrial Communications*, Ph.D. Dissertation, University of California, Los Angeles, 2000.

[9] R. Vaughan, N. Scott, and D. White, "The Theory of Bandpass Sampling," *IEEE Transactions on Signal Processing*, vol. 39, no. 9, pp. 1973–1984, September 1991.

[10] P. Baltus and R. Dekker, "Optimizing RF Front Ends for Low Power," *Proceedings of the IEEE*, vol. 88, no. 10, pp. 1546–1559, October 2000.

[11] T. Lee and S. Wong, "CMOS RF Integrated Circuits at 5 GHz and Beyond," *Proceedings of the IEEE*, vol. 88, no. 10, pp. 1560–1571, October 2000.

[12] H. Rategh, H. Samavati, and T. Lee, "A CMOS Frequency Synthesizer with an Injection-Locked Frequency Divider for a 5-GHz Wireless LAN Receiver," *IEEE Journal on Solid-State Circuits*, vol. 35, no. 5, pp. 780–787, May 2000.

[13] J.-K. Goo, K.-H. Oh, C.-H. Choi, Z. Yu, T. H. Lee, and R. W. Dutton, "Guidelines for the Power Constrained Design of a CMOS Tuned LNA," *Simulation of Semiconductor Processes and Devices, 2000*, SISPAD 2000 International Conference, Seattle, Washington, pp. 269–272, September 6008, 2000.

[14] R. Reedy, J. Cable, and D. Kelly, "Single Chip Wireless Systems Using SOI," *1999 IEEE International SOI Conference*, Rohnert Park, California, pp. 8–11, October 1999.

[15] M. Stuber, P. Dennies, G. Lyons, T. Kobayashi, and H. Domyo, "A Manufacturable SOI CMOS Process for Low Power Digital, Analog, and RF Applications," *1997 IEEE International SOI Conference*, Fish Camp, California, pp. 70–71, October 1997.

[16] M. Stuber, M. Megahed, J. Lee, T. Kobayashi, and H. Domyo, "SOI CMOS with High-Performance Passive Components for Analog, RF, and Mixed Signal Design," *1998 IEEE International SOI Conference*, Stuart, Florida, p. 99, October 1998.

[17] M. Megahed, M. Burgener, J. Cable, R. Benton, D. Staab, M. Stuber, P. Dennies, and R. Reedy, "Low Cost UTSI Technology for RF Wireless Applications," *1998 IEEE MTT-S Digest*, pp. 981–984, 1998.

[18] G. Lyons, "Commercial SOS Technology for Radiation-Tolerant Space Applications," *IEEE Radiation Effects Data Workshop 1998*, Newport Beach, California, pp. 96–99, July 1998.